Z. Phys. Chem. **220** (2006) 1407–1416 / **DOI** 10.1524/zpch.2006.220.10.1407

A Comparative Study on the Electronic Structure of the 1-Ethyl-3-Methylimidazolium Bis(trifluoromethylsulfonyl)amide RT-Ionic Liquid by Electron Spectroscopy and First Principles Calculations

By S. Krischok[1,*], R. Öttking[1], W. J. D. Beenken[1], M. Himmerlich[1], P. Lorenz[1], O. Höfft[2], S. Bahr[2], V. Kempter[2], and J. A. Schaefer[1]

[1] Institut für Physik und Institut für Mikro- und Nanotechnologien, TU Ilmenau, P.O. Box 100565, D-98684 Ilmenau, Germany
[2] Technische Universität Clausthal, Institut für Physik und Physikalische Technologien, Leibnizstr. 4, D-38678 Clausthal-Zellerfeld, Germany

(Received June 30, 2006; accepted August 10, 2006)

RT-Ionic Liquid / Electronic Structure / Density Functional Calculations / Photoelectron Spectroscopy (UPS, XPS) / Metastable Induced Electron Spectroscopy (MIES)

The near-surface electronic structure of the room-temperature ionic liquid 1-ethyl-3-methylimidazolium bis(trifluoromethylsulfonyl)amide has been investigated with ultraviolet and X-ray photoelectron spectroscopy as well as metastable induced electron spectroscopy. The results have been compared with density functional theory calculations. The good agreement between the experimental and theoretical data provides detailed insight into the origin of the observed spectral features. In particular, we found that a simple composition of the spectra of the isolated ions does not suffice to fit to the experimental results, but interionic interactions have to be considered.

1. Introduction

Room temperature ionic liquids (RT-ILs) have attracted much attention for their excellent properties, namely they remain in liquid phase over a wide temperature range, have very low vapor pressure at RT, are chemically inert,

* Corresponding author. E-mail: stefan.krischok@tu-ilmenau.de

and possess high heat capacities [1, 2]. These properties make them good candidates for the use in many fields [2, 3]. They may be used as "green" solvents [2], heat reservoirs [4], as well as electrolytes in electrochemical applications [5], homogeneous catalysis [2, 6, 7], and dye sensitized solar cells [8]. In order to refine the performance of RT-ILs, detailed knowledge of the geometric, electronic and vibronic structure of RT-ILs in the temperature regime between 100 K and 700 K appears indispensable. The need for vacuum-based studies employing surface analytical techniques has been pointed out recently [11].

A typical representative of RT-ILs is 1-ethyl-3-methylimidazolium bis(trifluoromethylsulfonyl)amide ([EMIM][Tf_2N]) [9, 10]. It can be distilled at moderate temperatures and reduced pressure, although the distillation rates are very low. In a previous study, we have applied ultraviolet and X-ray photoelectron spectroscopy (UPS (He I and II), XPS) as well as metastable induced electron spectroscopy (MIES) in order to study the electronic structure of [EMIM][Tf_2N] deposited on a polycrystalline Au substrate [12]. By combining UPS and XPS with MIES a wide range of depth resolution is covered. The depth resolution in photoelectron spectroscopy is defined by the inelastic mean free path of the emitted electron, whereas MIES is ultimately surface sensitive because the deexcitation of the He* takes place in front of the surface. The He atoms employed in MIES as probe atoms, are of thermal kinetic energy. Therefore they interact only with the outer edge of the charge density of the top layer at the ionic-liquid–vacuum interface [13, 14]. The interpretation of the collected data bases on previous studies on the electronic structure of 1-butyl-3-methylimidazolium bis(trifluoromethylsulfonyl)amide ([BMIM][Tf_2N]) among other RT-ILs by UPS using synchrotron radiation at 60 eV [1]. Applying density functional theory (DFT) in this study, the electronic structure of the RT-ILs was calculated for the two kinds of ions separately. By analysis of the Kohn–Sham molecular orbital energies, the density of states (DOS) for the cation and anion were determined, respectively. Each DOS has been shifted in energy as a whole until the superposition of both fit the measured spectral features of the RT-IL as good as possible. One of the strange results of this study is, that in contrast to what is usually found in ionic solids, *e.g.* NaCl, the surface states located at the valence band maximum (VBM) have been ascribed to molecular orbitals (MO) located on the organic cation. Thus, we have good reasons to assume that the procedure used in the mentioned study is not satisfactory for the understanding of the XPS and UPS spectra. Obviously, the specific interactions between anion and cation in the ionic liquid cannot be ignored. Therefore, we have performed density functional theory (DFT) calculations of the combined cation–anion complex, in order to gain a more realistic insight into the electronic structure of the ionic liquid [EMIM][Tf_2N].

2. Theoretical/experimental methods

2.1 Theoretical

We have performed DFT calculations using Becke's B3-LYP functional [15] and a 6-311G (3d, 2pd) basis set (as implemented in Gaussian03 [16]). The basis set extension by d-functions accounts for the hypervalent S=O bonds [17, 18]. The calculations, including structural optimization, were separately carried out for the isolated $[EMIM]^+$ cation and $[Tf_2N]^-$ anion as well as an complex formed of both. In the latter case we used as initial guess that at least one of the anions turns the carbon-tri-fluoride groups towards the cation. We found a minimum with a residual root mean square (RMS) force of 0.008 eV/Å. For the isolated ions the convergence was even better with a residual RMS force below 0.00002 eV/Å. For the relaxed structures, we determined the Kohn–Sham eigenenergies and MOs. Assuming uniform crosssections per eigenstate and a Gaussian broadening of 0.8 eV we convolute the calculated eigenstates to a DOS comparable to the experimental spectra.

Additionally, the calculated and plotted Kohn–Sham MOs allow us to localize the origin of the emitted electrons assigned to different subbands in the XPS, UPS and MIES spectra.

We have to concede that all our calculations are not fully adequate to describe the [EMIM][Tf_2N] system in liquid but rather in gas phase. Thus, solvation effects are not considered at the present stage of our calculations. For the cation–anion complex, Coulomb interaction and hydrogen-bonds between the ions are only considered for the two ions forming the specific cation–anion complex. For these reasons and the very slow relaxation of ions, some uncertainties in the actual molecular structure of the ions and their orientation in the complex remain. However, one will see that this has only minor impact on the DOS of the cation–anion complex, despite of a uniform shift of the calculated energies of about +1.35 eV to fit the experimental data. We may note that explaining this shift to higher energies by the Madelung-energy, which usually results in lower actual energies, is a problem and very complicated due to the ionic character of the solvent.

2.2 Experimental

For our experimental studies two UHV systems (base pressure below 2×10^{-10} Torr), both equipped with XPS and UPS (He I and II, photon energies 21.2 eV and 40.8 eV, respectively), have been used (see also Ref. [12]). Thus, a cross referencing of the collected data on the different systems is easily possible.

The first apparatus was used for photoelectron spectroscopy by combining UPS (He I and II) and monochromated XPS (Al K_α). It features an energy resolution below 0.6 eV (on Ag3$d_{5/2}$ at a pass energy of 15 eV) for XPS, while

a resolution below 150 meV (as estimated from the Fermi edge of a polycrystalline Ag sample) has been employed for the UPS measurements. The emitted electrons are collected using a hemispherical analyzer equipped with 7 channeltrons. Thus, the apparatus provides excellent conditions for the measurement of high quality spectra.

The second apparatus is additionally equipped with a source for metastable He atoms. This source is suited for performing MIES and UPS (He I) measurements in parallel. Experimental details of the apparatus can be found in Refs. [19–21]. A gas discharge produces metastable He atoms with about 20 eV potential energy, but only thermal kinetic energy, as well as He I photons for UPS (He I). Metastable atoms (He* $2^3S/2^1S$ with 19.8/20.6 eV excitation energy, respectively, and an intensity ratio of about 7 : 1) of thermal kinetic energy (60 to 100 meV) approach the surface, and the electron exchange processes with the species of the surface (resonant electron exchange and Auger processes) take place well in front of the surface (0.2 nm, typically). In this study, the electron emission is due to Auger deexcitation of $He^*(2^3S)$ (see also Section 3.2), and the spectra of the emitted electrons provide a rather direct image of the DOS of the initially filled electronic states. For more detailed introductions into MIES and its various applications in molecular and surface spectroscopy see Refs. [13, 14, 22]. The spectral analysis was made with a hemispherical analyzer, and all spectra possess an energy resolution of about 250 meV.

The sample support consists of a polycrystalline Au film of about 250 nm thickness deposited on Si(100), separated by a Ti adhesion layer. The samples were prepared by depositing one droplet of the ultra-pure RT-IL onto the Au substrate, and were, after careful outgasing in a load lock system, introduced into the UHV chamber. The liquid [EMIM][Tf_2N] samples prepared in this way have very low vapor pressure, and no change of the base pressure could be detected during the measurements performed at RT.

After the introduction of the RT-IL into the UHV chamber, the sample was first characterized by monochromated XPS (Al K_α). The survey spectra indicate that a closed RT-IL film was successfully prepared. From the absence of any substrate (Au) related spectral feature in the XPS spectra, we estimate a film thickness of more than 10 nm in both cases. The expected elements F, N, O, S, and C are detected, and no evidence of impurities by other elements could be found. A calculation of the chemical composition based on the observed peak areas leads to values close to the expected ones. The F(1*s*), N(1*s*), O(1*s*), S(2*s*), and C(1*s*) emissions display well-resolved and narrow spectral features with the expected chemical shifts and relative peak areas. A more detailed discussion of the XPS spectra typical for the [EMIM][Tf_2N] film can be found elsewhere [12].

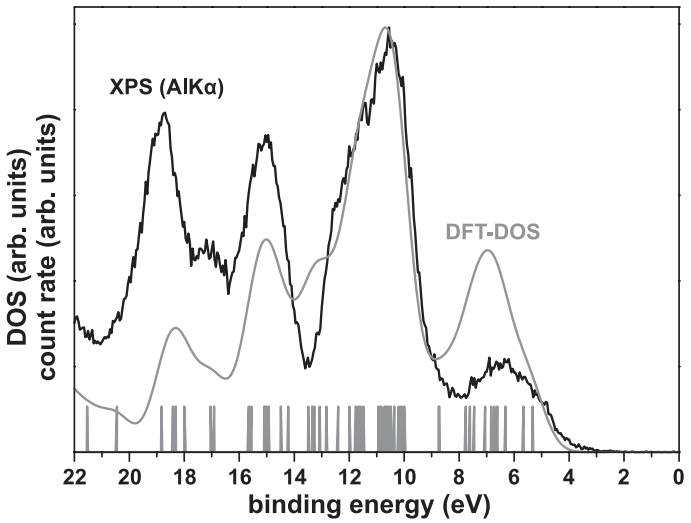

Fig. 1. Comparison of eigenstates and convoluted DOS of the [EMIM][Tf_2N] complex as calculated by DFT (grey) in comparison to the corresponding XPS spectrum (black). Energy values obtained by DFT have been shifted by 1.35 eV as described in the text.

3. Results and discussion

3.1 Theoretical and XPS results

The optimization of the cation–anion complex structure by our DFT calculations results in a binding energy of $E_B = 6.53$ eV. This has been calculated as the difference of the total energy of the complex (−59 112 eV) and those of the relaxed anion (−49 666 eV) and cation (−9271 eV).

In the resulting configuration (see Fig. 2) the $[Tf_2N]^-$ anion is situated above the imidazolium ring, with the CF_3 groups facing towards the $[EMIM]^+$ cation. The distance between the centre of the imidazolium ring and the C-atom of the closer CF_3 group is about 3.75 Å. Furthermore, the distance between the C-atoms of the ethyl group of the $[EMIM]^+$ cation and the nearest F-atom of the other CF_3 group is 3.41 Å and 3.54 Å, respectively.

The Mulliken population analysis for the complex yields a charge of −0.87 eV on the $[Tf_2N]^-$ anion and consequently +0.87 eV on the $[EMIM]^+$ cation. This applies for the almost ionic character of the [EMIM][Tf_2N] complex, despite a calculated charge density overlap of 0.13 eV.

The calculated DOS of the [EMIM][Tf_2N] complex, shifted uniformly by about 1.35 eV towards lower binding energies and convoluted using Gaussians with a characteristic width of 0.8 eV, is shown together with our experimental XPS data (see Fig. 1). For the energy shift and the normalization of the calculated spectrum we aimed to match the most prominent peak in the XPS spectrum at 10–12 eV. As mentioned above, this shift most probably accounts

for the interaction to other ions in the liquid environment of the complex, which we could not consider in our DFT calculations. However, a slight surface charging leading to an artificial shift towards lower energies cannot be ruled out completely, but is rather unlikely since the measured binding energies by MIES, UPS, and XPS are identical. It is important to note, that indeed for UPS (He I) measurements with high photon fluxes a slight shift of the spectra (up to 0.8 eV) was observed.

Including the mentioned energy shift and broadening, our calculation gives a remarkable agreement between experimental and theoretical data. The HOMO energy, which represents the valence band edge, is given as 5.5 eV with respect to the vacuum level. The corresponding Kohn–Sham MO is shown in Fig. 2 (A, C). Interestingly, like the most of the other MOs belonging to states in the upper valence band (from 5.5 eV to 7.8 eV), it is located on the $[Tf_2N]^-$ anion. This result is exactly what one expects from intuition, *i.e.* low energy photoelectrons should be emitted from the anion, but contradicts previous considerations based on calculations using the method of ion spectra superposition [1, 12].

The states located on the $[EMIM]^+$ cation in the complex, which are closest to the valence band edge, are the 10^{th} and 12^{th} below HOMO. They correspond to the HOMO and HOMO-1 of the isolated $[EMIM]^+$ cation, respectively, as one may see for the former by comparing the MOs shown in Fig. 2 panels E and F. In the cation–anion complex, these states are quite hidden among the states localized on $[Tf_2N]^-$ anion.

Next, we find the most pronounced spectral feature of the XPS spectrum between 9.5 eV and 12.5 eV binding energy. The corresponding MOs show a delocalization among the $[EMIM]^+$ cation and the fluorines of the anion, the latter with strong non-bonding character. This may account for the partial charge density overlap mentioned above and the specific orientation of the ions in the complex.

In the calculated DOS, a shoulder appears around 13 eV, which is not found in the XPS spectrum. The corresponding MOs are located on the $[EMIM]^+$ cation with significant contributions on the attached alkyl groups. Due to the mentioned structural uncertainties, these groups may be differently oriented and consequently the state-energies are uncertain as well. On the other hand, the energies of these MOs are not that much sensitive to conformational changes that a reordering of the bands will be necessary. Thus these states may correspond to the shoulder of the prominent peak found at 12.5 eV in the XPS spectrum.

The band around 15 eV is a band of states located almost exclusively on the $[Tf_2N]^-$ anion. Even for deeper bands down to 20 eV the calculated DOS still fits to the XPS spectrum. Taking into account this excellent agreement between the calculated DOS and the XPS data at least for peak positions, we may trust in the DFT calculations on the $[EMIM][Tf_2N]$ complex. Hartree–Fock based calculations (not shown) failed in this respect completely.

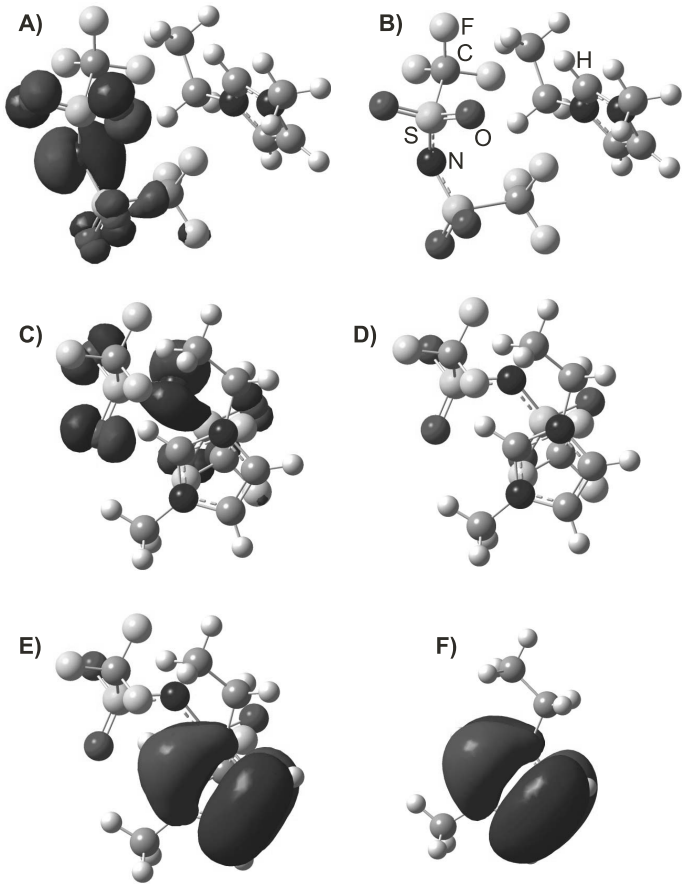

Fig. 2. Visualization of selected MOs and of the mutual structural positions: **A**, **C** the HOMO in side- and front-view with the $[EMIM]^+$ cation at the right in **A** and facing to the front in **C**, respectively. **B**, **D** the corresponding atomic skeletons to clarify the molecular structure of the gas-phase molecule. The lowest panels show the comparison of the highest $[EMIM]^+$ MO (=HOMO-10) in the [EMIM][Tf_2N] complex **E** with the HOMO of the isolated $[EMIM]^+$ cation **F**.

3.2 UPS and MIES

The qualitative agreement of the MIES and photoelectron spectroscopy data (see Fig. 3), as far as the position of the spectral features is concerned, allows us to conclude directly, that the electron emission is due to $He^*(2^3S)$ interacting with the surface *via* the Auger deexcitation process. Consequently, the MIES spectra reflect the DOS of the electronic states located on the vacuum side of the vacuum–liquid interface (about 0.2 nm in front of the surface). From the

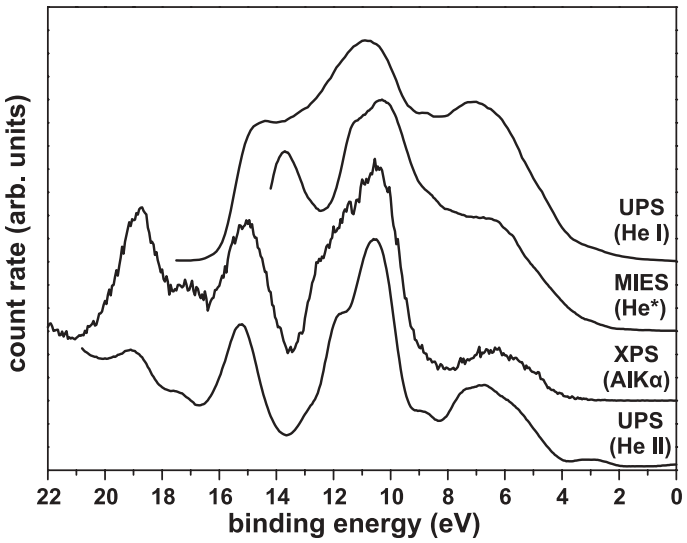

Fig. 3. Valence band spectra obtained by various spectroscopic techniques. From top to bottom: UPS (He I), MIES, XPS, and UPS (He II).

high energy cut-off of the MIES and UPS (He I) spectra, a work function of about 5.0 ($\pm$0.2) eV is determined, if charging is absent.

The remarkable overall similarity of the spectra obtained with several valence band spectroscopies of widely different information depth, including XPS (see Fig. 3), suggests that the surface electronic structure of the IL is, at 300 K, rather similar to that of the bulk, at least over the thickness covered by the information depth of XPS. The minor deviations between the spectra provided by the different techniques can be traced back to different information depths, cross sections for electron ejection (photoionization *versus* Auger emission) and final state effects (the latter occurring in the photoelectron spectroscopies, only).

Comparing the UPS (He II) with the XPS spectra we found a far less pronounced band between 12 eV and 13 eV and small additional features at about 9 eV and 3 eV, respectively. The latter originate from He II β and γ contributions and, therefore, cannot be assigned to additional electronic states of the RT-IL. As mentioned above, according to our calculations the states between 12 eV and 13 eV are related to MOs located at the imidazolium ring as well as at the alkyl groups of the $[EMIM]^+$ cation, which bare some uncertainty due to structural uncertainties (see Sections 2.1 and 3.1). Thus, a detailed explanation of the minor differences between the XPS and UPS spectra is not available at present, and will be subject of future investigations.

As compared to XPS and UPS (He II), the emission seen in the region between 4 eV and about 9 eV is more pronounced in the MIES spectra (if

spectra are normalized to the most intense structure at about 10 eV) while the dip at about 8 eV appears less pronounced. According to our calculations, in this energy range the emission from the highest MOs, localized at the $[EMIM]^+$ cation mainly, contributes (see Fig. 2, panel E). These MOs possess π-character. Thus, we assume that the reason for the intensity enhancement seen with MIES in this energy region has its origin in the shape of the responsible MOs which may enhance the probability for the Auger deexcitation process involving these MOs.

4. Summary

We have studied the valence band structure of the room-temperature ionic liquid [EMIM][Tf_2N] by XPS, UPS and MIES and compared the spectra to DFT calculations. We found excellent agreement, which enables us to identify the different subbands. Most notably, the valence band maximum is attributed to the HOMO of the $[Tf_2N]^-$ anion within the [EMIM][Tf_2N] complex in contrast to what is found by simple combination of the DOS of the separated $[EMIM]^+$ and $[Tf_2N]^-$ ions. Therefore, we believe that such an approach does not provide a sufficiently accurate model due to missing interionic interactions and the entire cation–anion system has to be considered in theoretical calculations. Nevertheless, the experimental methods are sensitive to the different localization of the states on cation and anion in the combined system. Even a coarse assignment of the states in the DOS to the localization of the corresponding MOs enables an improved understanding of the spectra obtained by XPS, UPS, and MIES. A more detailed analysis of the differences emerging from these various spectroscopies has to consider the structure of the particular MOs and will be subject of future studies.

Acknowledgement

We are grateful to F. Endres (Clausthal University of Technology) for the supply of the RT-IL samples and his continuous interest in this work.

References

1. D. Yoshimura, T. Yokoyama, T. Nishi, H. Ishii, R. Ozawa, H. Hamaguchi, and K. Seki, J. Electron Spectrosc. Relat. Phenom. **144–147** (2005) 319.
2. P. Wasserscheid and W. Keim, Angew. Chem. **112** (2000) 3926.
3. K. Binnemans, Chem. Rev. **105** (2005) 4148.
4. J. M. Crosthwaite, M. J. Muldoon, J. K. Dixon, J. L. Anderson, and J. F. Brennecke, J. Chem. Thermodyn. **37** (2005) 559.
5. F. Endres and S. Z. El Abedin, Phys. Chem. Chem. Phys. **8** (2006) 2101.
6. P. Kölle and R. Dronskowski, Inorg. Chem. **43** (2004) 2803.
7. T. Welton, Chem. Rev. **99** (1999) 2071.

8. C. Pinilla, M. G. Del Popolo, R. M. Lynden-Bell, and J. Kohanoff, J. Phys. Chem. B **109** (2005) 17922.
9. L. P. N. Rebelo, J. N. C. Lopes, J. M. S. S. Esperanca, and E. Filipe, J. Phys. Chem. **109** (2005) 6040.
10. M. J. Earle *et al.*, Nature **439** (2006) 831.
11. J. Dupont and P. A. Z. Suarez, Phys. Chem. Chem. Phys. **8** (2006) 2441.
12. O. Höfft, S. Bahr, M. Himmerlich, S. Krischok, J. A. Schaefer, and V. Kempter, Langmuir **22** (2006) 7120.
13. Y. Harada, S. Masuda, and H. Ozaki, Chem. Rev. **97** (1997) 1897.
14. H. Morgner, Adv. Atom. Mol. Opt. Phys. **42** (2000) 387.
15. A. D. Becke, J. Chem. Phys. **98** (1993) 5648.
16. M. J. Frisch *et al.*, Gaussian 03, Revision C.02, Gaussian, Inc., Wallingford CT (2004).
17. A. D. McLean and G. S. Chandler, J. Chem. Phys. **72** (1980) 5639.
18. R. Krishnan, J. S. Binkley, R. Seeger, and J. A. Pople, J. Chem. Phys. **72** (1980) 650.
19. W. Maus-Friedrichs, M. Wehrhahn, S. Dieckhoff, and V. Kempter, Surf. Sci. **237** (1990) 257.
20. P. Stracke, S. Krischok, and V. Kempter, Surf. Sci. **473** (2001) 86.
21. S. Krischok, O. Höfft, J. Günster, J. Stultz, D. W. Goodman, and V. Kempter, Surf. Sci. **495** (2001) 8.
22. J. Günster, S. Krischok, V. Kempter, J. Stultz, and D. W. Goodman, Surf. Rev. Lett. **9** (2002) 1511.